6

Theoretical Analysis on Smith-Purcell Free-Electron Laser

D. Li[1], M.Hangyo[2], Y. Tsunawaki[3], Z. Yang[4], Y. Wei[4],
S. Miyamoto[5], M. R. Asakawa[6] and K. Imasaki[1]
[1]*Institute for Laser Technology*
[2]*Osaka University*
[3]*Osaka Sangyo University*
[4]*University of Electronic Science and Technology of China*
[5]*University of Hyogo*
[6]*Kansai University*
[1,2,3,5,6]*Japan*
[4]*China*

1. Introduction

The first observation of radiation emitted by an electron passing over a diffraction grating was made long ago by Smith and Purcell [Smith, S. J.], and the idea of using this effect in a free-electron laser has been proposed by numerous authors [Gover, A., Schachter, L., Leavitt, R.P.], and a cavity is usually used to provide feedback in those schemes. A renewed interest in Smith-Purcell radiation has been raised in recent years, since the analysis of the dispersion relation of surface waves for lamellar gratings by Andrews and Brau [Andrews, H.]. They pointed out that the interaction between an initially continuous electron beam and a surface wave on the grating could lead to bunching at the frequency of the wave, and subsequently the periodic electron bunches induce strong radiation at a certain angle, and it is called super-radiant Smith-Purcell radiation. Thus, the Smith-Purcell radiation is recongnized to be a promising alternative in the development of a compact, tunable and high power terahertz device. The terahertz sources, a currently active research area, are of importance in a variety of applications to biophysics, medical and materials science.

It is well known that the Smith-Purell radiation is emitted as an electron passes close to the surface of a periodic metallic grating. The incoherent Smith-Purcell radiation has been analyzed in many ways, such as diffraction theory, integral equation method and induced surface current model [van den Berg, P.M., Walsh, J., Shibata, Y.]. The super-radiant Smith-Purcell radiation is regarded as the result of the periodic electron bunches, which can be generated from a system of pre-bunched beam, or the interaction of initial continuous beam with the enhanced surface wave traveling along the grating. Several theories have been proposed to explain the super-radiant phenomenon and calculate the growth rate of the radiation[Kuma, V., Schächter, L, Andrews. H.]. With particle-in-cell simulations, the incoherent, coherent and super-radiant Smith-Purcell radiation have been demonstrated,

and some ideas on improvement of the gorwth rate were proposed [Donohue, J.T.,Li, D.]. Recently, experiments of proof-of-principal are carried out [Andrews, H., Gardelle, J.], and the experimental results are in agreement with the theoretical analysis.

In this Chapter, we introduce the Smith-Purcell free-electron lasers through theoretical analysis and particle-in-cell simulation. We are trying to understand the incoherent and superradiant Smith-Purcell radiation by a complete calculation of a single electron bunch, a train of bunches and a continuous beam, respectively. Some proposals on enhanceing the interaction of electron beam with surface waves are demonstrated. We also explore the characterics of the Smith-Purcell radiation from a grating made of negative-index materials.

2. Theory of grating emission

When an electric charge moves, at constant speed, parallel to a grating, it excites Smith-Purcell radiation and surface wave. The surface wave is not radiant, unless it comes to the ends of the grating. It partially reflects and diffracts there, and the part of diffraction is radiant. In this secetion, we theoretically analyze the two phenomena.

2.1 Smith-Purcell radiation

We consider a two-dimensional scheme of lamellar grating made of perfect conductor embedded in vacuum as shown in Fig. 1. The periodicity of the grating is chosen in the z direction, whereas the grating's rulings are parallel to the y axis. We consider the idealized case that a line charge is supposed to pass over the grating along the z axis. The single

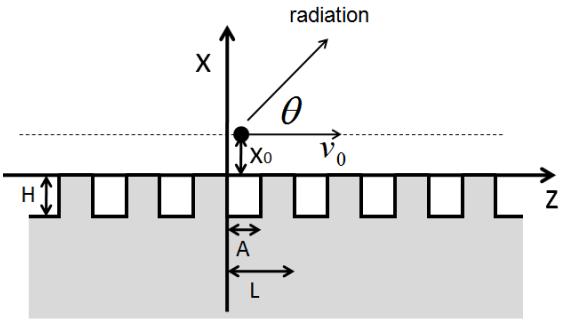

Fig. 1. Cross section of the configuration. Rectangular grating; A=groove width, H=groove depth, L=period.

line charge, with a charge-density distribution q per unit length in the y direction, moves with velocity v_0 along the trajectory $x = x_0$. Both the geometry of the configuration and all field quantities are independent of y direction since it is two dimensional. Thus, the expression for the current density of the line charge can be written as

$$J_z(x,z,t) = qv_0\delta(x - x_0)\delta(z - v_0 t) \tag{2.1}$$

The Fourier transform of the current density is then given by

$$J_z(x,z,\omega)=\int_{-\infty}^{\infty}J_z(x,z,t)e^{j\omega t}dt=q\delta(x-x_0)e^{j\frac{\omega}{v_0}z} \tag{2.2}$$

The current distribution described by Eq. (2.2) excites the z-directed component of the magnetic vector potential which in turn satisfies

$$(\frac{\partial^2}{\partial x^2}+\frac{\partial^2}{\partial z^2}+\frac{\omega^2}{c^2})A_z(x,z,\omega)=-\mu_0 J_z(x,z,\omega) \tag{2.3}$$

Its solution is assumed to have the form $A_z(x,z,\omega)=A_z(x,\omega)e^{j\frac{\omega}{v_0}z}$, and $A_z(x,\omega)$ satisfies

$$(\frac{d^2}{dx^2}-\frac{\omega^2}{v_0^2}+\frac{\omega^2}{c^2})A_z(x,\omega)=-\mu_0 q\delta(x-x_0) \tag{2.4}$$

For $x>x_0$ the solution of this equation is

$$A_z(x>x_0,\omega)=C_+e^{-\alpha_0(x-x_0)},$$

and for $x<x_0$

$$A_z(x<x_0,\omega)=C_-e^{\alpha_0(x-x_0)},$$

where $\alpha_0^2=(\omega/v_0)^2-(\omega/c)^2$. The $A_z(x,\omega)$ should be continuous at $x=x_0$, thus we have $C_+=C\_=C$, whereas its derivative is discontinuous. The discontinuity is determined by the Dirac delta function in Eq. (2.4), therefore by integrating Eq. (2.4) we obtain

$$[\frac{d}{dx}A_z(x)]_{x=x_0^+}-[\frac{d}{dx}A_z(x)]_{x=x_0^-}=-\mu_0 q,$$

hence

$$-\alpha_0 C-\alpha_0 C=-\mu_0 q,$$

Then we get

$$C=\frac{\mu_0 q}{2\alpha_0}.$$

We conclude that the magnetic vector potential reads

$$A_z(x,z,\omega)=\frac{\mu_0 q}{2\alpha_0}e^{-\varepsilon(x)\alpha_0(x-x_0)}e^{j\frac{\omega}{v_0}z},$$

where $\varepsilon(x)=-1$ for $x<x_0$, and $\varepsilon(x)=1$ for $x>x_0$. The magnetic field of y component can be obtained as

$$H_y(x,z,\omega) = -\frac{1}{\mu_0}\frac{\partial A_z(x,z,\omega)}{\partial x} = \frac{q\varepsilon(x)}{2} e^{-\varepsilon(x)\alpha_0(x-x_0)} e^{j\frac{\omega}{v_0}z},$$

and the incident field on the grating surface should be $H_y^i = -\frac{q}{2} e^{\alpha_0(x-x_0)} e^{j\frac{\omega}{v_0}z}$.

Above the grating we expand the reflected fields H_y^r in Floquet series (space harmonics), and the total magnetic field can be written as

$$H_y^T = H_y^i + H_y^r = -\frac{q}{2} e^{\alpha_0(x-x_0)} e^{j\frac{\omega}{v_0}z} + \sum_{p=-\infty}^{\infty} A_p e^{j\alpha_p x} e^{jk_p z}, \tag{2.5}$$

where $k_p = \omega/v_0 + 2\pi p/L$, $\alpha_p^2 = (\omega/c)^2 - k_p^2$, and A_p is the scalar coefficient to be determined. It is clear that, the refracted waves are evanescent for $p \geq 0$, since α_p is imaginary; when p is negative integer, some of the refracted modes radiate in a certain range of frequency to guarantee $\alpha_p^2 > 0$. The frequency range is worked out, and we express it in wavelength

$$\frac{L}{|p|}\left(\frac{1}{\beta} - 1\right) \leq \lambda \leq \frac{L}{|p|}\left(\frac{1}{\beta} + 1\right).$$

Then, we can define an angle of emergence θ ,between the radiating wave and the charge moving direction. Thus, from the relation $k_p = (\omega/c)\cos\theta = \omega/v_0 + 2\pi p/L$, it is straightforward to achieve

$$\lambda = \frac{L}{|p|}\left(\frac{1}{\beta} - \cos\theta\right), \tag{2.6}$$

which is well known for Smith-Purcell radiation.

The z-directed electric field can be obtained from Eq.(2.5) by using the Maxwell equations, and it reads

$$E_z^T = \frac{j}{\omega\varepsilon_0}\left(-\frac{q\alpha_0}{2} e^{\alpha_0(x-x_0)} e^{j\frac{\omega}{v_0}z} + \sum_{p=-\infty}^{\infty} jA_p\alpha_p e^{j\alpha_p x} e^{jk_p z}\right) \tag{2.7}$$

For simplicity without sacrificing the generality, only the lowest mode in the groove, which is the most easily excited mode, is considered. Its electromagnetic fields are given by

$$H_y^g = B\left(\cos\left(\frac{\omega}{c}x\right) + \tan\left(\frac{\omega}{c}H\right)\sin\left(\frac{\omega}{c}x\right)\right), \tag{2.8}$$

$$E_z^g = \frac{-j}{c\varepsilon_0} B\left(\sin\left(\frac{\omega}{c}x\right) + \tan\left(\frac{\omega}{c}H\right)\cos\left(\frac{\omega}{c}x\right)\right), \tag{2.9}$$

where B is a scalar coefficient to be determined.

At the surface of the grating ($x=0$) the tangential component of the electric field is continuous. Since the tangential field vanishes on the surface of the conductor, we get

$$E_z^T(x=0)=\begin{cases}E_z^g(x=0) & for 0\le z\le A\\ 0 & for A\le z\le L\end{cases}. \tag{2.10}$$

We multiply by $e^{-jk_r z}$ and integrate over $0<z<L$, we get

$$A_r=\frac{j}{2\alpha_r L}\left(\frac{2B\omega}{c}\tan\left(\frac{\omega}{c}H\right)\psi_1^r-q\zeta\alpha_0 L e^{-\alpha_0 x_0}\delta_{r,0}\right), \tag{2.11}$$

where $\psi_1^r=\int_0^A e^{-jk_r z}dz$. Likewise, the tangential component of the magnetic field must be continuous at the grating surface,

$$H_y^T(x=0)=H_y^g(x=0). \tag{2.12}$$

We integrate over $0<z<A$, and we get

$$B=\frac{1}{A}\left(\sum_{p=-\infty}^{\infty}A_p\psi_2^p-\frac{1}{2}qe^{-\alpha_0 x_0}\psi_2^0\right), \tag{2.13}$$

where $\psi_2^p=\int_0^A e^{jk_p z}dz$. If we change r in Eq. (2.11) by p and substitute it into Eq. (2.13), we get

$$B=-\frac{1}{2}\frac{q\psi_2^0(j+1)L}{e^{\alpha_0 x_0}\left(-j\frac{\omega}{c}\tan\left(\frac{\omega}{c}H\right)\left(\sum_{p=-\infty}^{\infty}\frac{\psi_1^p\psi_2^p}{\alpha_p}\right)+AL\right)}. \tag{2.14}$$

Substitute Eq.(2.14) into Eq.(2.11), we finally get the expression for coefficients of reflected waves,

$$A_r=j\frac{1}{2\alpha_r L}\left(-\frac{q\psi_2^0(1+j)L\frac{\omega}{c}\tan\left(\frac{\omega}{c}H\right)\psi_1^r}{e^{\alpha_0 x_0}\left(-j\frac{\omega}{c}\tan\left(\frac{\omega}{c}H\right)\left(\sum_{p=-\infty}^{\infty}\frac{\psi_1^p\psi_2^p}{\alpha_p}\right)+AL\right)}-q\alpha_0 L e^{-\alpha_0 x_0}\delta_{r,0}\right). \tag{2.15}$$

In order to be independent of influence from the charge, we define

$$A_r^u=\frac{A_r}{qe^{-\alpha_0 x_0}}=j\frac{1}{2\alpha_r L}\left(-\frac{\psi_2^0(1+j)L\frac{\omega}{c}\tan\left(\frac{\omega}{c}H\right)\psi_1^r}{-j\frac{\omega}{c}\tan\left(\frac{\omega}{c}H\right)\left(\sum_{p=-\infty}^{\infty}\frac{\psi_1^p\psi_2^p}{\alpha_p}\right)+AL}-\alpha_0 L\delta_{r,0}\right). \tag{2.16}$$

So, the coefficients of reflected waves can be numerically calculated when relevant parameters are given.

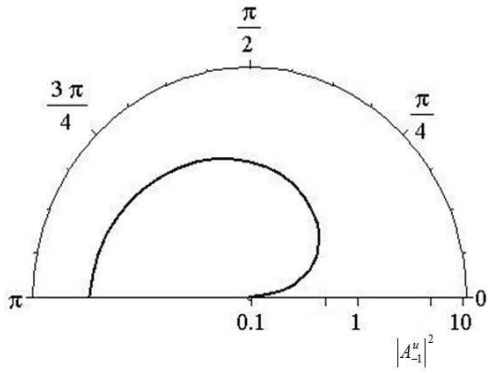

Fig. 2. Radiated intensity $\left|A^u_{-1}\right|^2$ in the -1st order Smith-Purcell radiation as a function of the radiating angle.

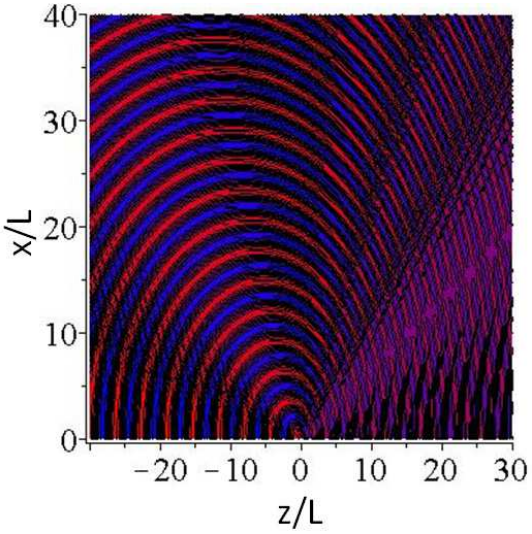

Fig. 3. Contour plot of the magnetic field of -1st order Smith-Purcell radiation H_y^{-1}.

The grating to be calculated is with the parameters, L=173 μ m, A=62 μ m, and H=100 μ m. The electron energy is 40 keV. We focus on the –1st order($p=-1$) wave, which is the lowest mode. Only the radiating waves (Smith-Purcell radiation) are considered, so we substitute Eq.(2.6) into Eq.(2.16), and calculate the dependency of radiated intensity $\left|A^u_{-1}\right|^2$ on the emission angle θ. The results are given in Fig.2. It is shown that the Smith-Purcell radiation induced by a single line charge is dependent on the radiation angle, and the backward radiation is stronger than the forward radiation. Remember that the radiation wave length and the radiation angle satisfy the Eq. (2.6), so, the wave length of the backward radiation is longer than that of the forward one. The –1st order refracted magnetic field is expressed as

$$H_y^{-1} = A_{-1}^u e^{j\alpha_{-1}x} e^{jk_{-1}z}. \tag{2.17}$$

Based on Eq. (2.17), the space distribution of H_y^{-1} can be calculated, and the contour plots are given in Fig.3.

2.2 Surface wave

Considering the case of abscence of electric charge in Fig. 1, we search the evenescent mode on the surface of the grating . Our analysis focuses on the transverse magnetic wave mode, which has longitudinal electric field. The y-directed component of the magnetic field above the grating ($x > 0$) can be expanded in Floquet series, and it is written as

$$H_y^a = \sum_{p=-\infty}^{\infty} A_p e^{-\alpha_p x} e^{jk_p z}, \tag{2.18}$$

where $k_p = k + 2\pi p/L$, $\alpha_p^2 = k_p^2 - (\omega/c)^2$, and A_p is the scalar coefficient to be determined. The z-directed electric field can be obtained from Eq.(2.18) by using the Maxwell equations, and it reads

$$E_z^a = \frac{-j}{\omega\varepsilon_0} \sum_{p=-\infty}^{\infty} A_p \alpha_p e^{-\alpha_p x} e^{jk_p z} \tag{2.19}$$

As mentioned above, only the lowest mode in the groove ($0 > x > -H$), which is the most easily excited mode, is considered. Its electromagnetic fields are same to Eq.(2.8) and Eq. (2.9), and we write here again

$$H_y^g = B(\cos(\frac{\omega}{c}x) + \tan(\frac{\omega}{c}H)\sin(\frac{\omega}{c}x)) \tag{2.20}$$

$$E_z^g = \frac{-j}{c\varepsilon_0} B(\sin(\frac{\omega}{c}x) + \tan(\frac{\omega}{c}H)\cos(\frac{\omega}{c}x)) \tag{2.21}$$

where B is scalar coefficient to be determined.

At the surface of the grating ($x = 0$) the tangential component of the electric field is continuous. Since the tangential field vanishes on the surface of the conductor, we get

$$E_z^a(x=0) = \begin{cases} E_z^g(x=0) & for 0 \le z \le A \\ 0 & for A \le z \le L \end{cases}$$

We multiply by $e^{-jk_q z}$ and integrate over $0 < z < L$, we get

$$A_q \alpha_q L = \frac{\omega}{c} B \tan(\frac{\omega}{c}H)\psi_1^q \tag{2.22}$$

where $\psi_1^q = \int_0^W e^{-jk_q z} dz$. Likewise, the tangential component of the magnetic field must be continuous at the grating surface,

$$H_y^a(x=0) = H_y^g(x=0) .$$

We integrate over $0 < z < A$, and we get

$$BA = \sum_{p=-\infty}^{\infty} A_p \psi_2^p , \tag{2.23}$$

where $\psi_2^p = \int_0^A e^{jk_p z} dz$. If we change q in Eq. (2.11) by p and substitute it into Eq. (2.23), we get the dispersion equation for the surfave wave

$$1 = \sum_{p=-\infty}^{\infty} \frac{\omega \tan(\frac{\omega}{c} H) \psi_1^p \psi_2^p}{\alpha_p LAc} . \tag{2.24}$$

With the parameters mentioned above, L=173 μ m, A=62 μ m, and H=100 μ m, Eq.(2.24) is calculated and the result is shown in Fig.4. This is a typical dispersion curve for a slow-wave structure. In the region $0 < kL/2\pi < 0.5$, the phase velocity is in the same direction of the group velocity, and it is called tarvelling wave. In the region $0.5 < kL/2\pi < 1$, the phase velocity and the group velocity are in opposite directions, and it is called backward wave. A beam line for 40 keV electron beam is also plotted in Fig. 4. The beam line interacts with the backward wave, thus, the electromagnetic energy flows opposite to the beam moving direction and form the backward wave oscillator, which external feedback is not necessary.

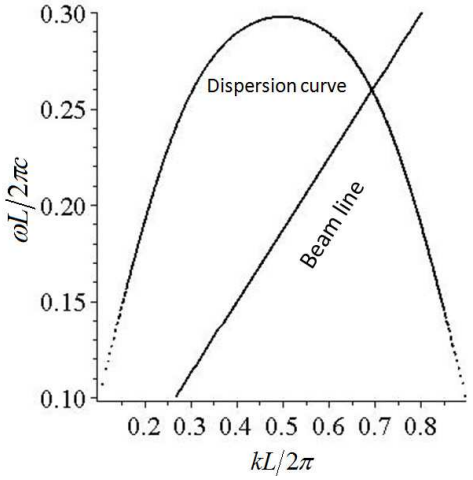

Fig. 4. Dispersion relation of the surface wave of the grating with parameters L=173 μ m, A=62 μ m, and H=100 μ m. The beam line is for 40 keV electron beam.

3. Simulation of grating emission

The particle-in-cell code employed in our simulation, MAGIC, is developed by Mission Research Corporation. It is a finite-difference, time-domain code for simulating processes that involve interactions between space charge and electromagnetic fields.

We consider a two-dimensional model consisting a grating with rectangular form, a sheet electron beam and vacuum region for electron-wave interaction and radiation propagation. The simulation geometry is as shown in Fig. 5, where the grating is set in the center of the bottom of the vacuum box. The simulation uses the Cartesian coordinate system, with the origin being chosen at the center of the grating. The surface of the grating is assumed to consist of a perfect conductor whose grooves are parallel and uniform in the y direction. The electron beam is chosen as the sheet form, with a finite thickness. The beam, a perfect laminar beam produced by the MAGIC algorithm and moving in the *z*-axis, is generated from a cathode, which is located at the left boundary of the simulation box and 34μm above the grating. The vacuum box is bordered with a special region (called *free-space* in MAGIC language), in which incident electromagnetic waves and electrons can be absorbed. The whole simulation area is divided into mesh with rectangle cell of very small size in the region of beam propagation and large size in the remainder. Since it is a two-dimensional simulation, it assumes that all fields and currents are independent of the z coordinate, and it should be noted that the current value mentioned in the paper represents the current per meter in the z direction.

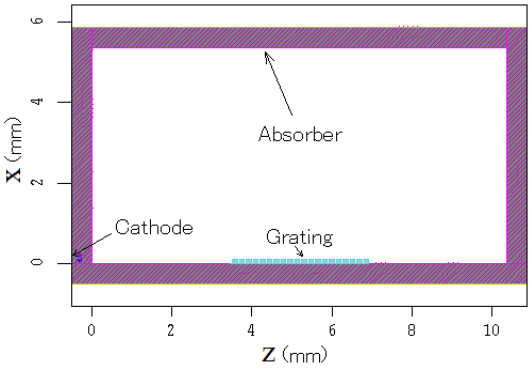

Fig. 5. Geometry used in simulation. (The surface of the grating is assumed to consist of a perfect conductor)

grating period	173 μm
groove width	62 μm
groove depth	100 μm
electron beam energy	40 keV
beam thickness	24 μm
beam-grating distance	34 μm
external magnetic field	2 T

Table 1. Main parameters for simulation

The main parameters chosen in our simulation are summarized in table 1. The electron beam specification will be varied and described in detail in each of the following simulation cases when it is necessary. The external magnetic field (z direction) is only used for the continuous beam simulation, in order to ensure stable beam propagation above the grating.

As to the diagnostics, MAGIC allows us to observe a variety of physical quantities such as electromagnetic fields as functions of time and space, power outflow, and electron phase-space trajectories . We can set the relevant detectors anywhere in the simulation area.

3.1 A single bunch

First of all, we simulate a single electron bunch passing over a grating possessing 20 periods, so as to clearly observe the radiation process. The electron beam current is 480 mA, and the bunch is 0.1 ps long, small compared to the Smith-Purcell radiation wavelength allowed by Eq. (2.6), and consequently the radiation is coherent. The code runs enough time to ensure that all the radiation emitted arrive at the detector.

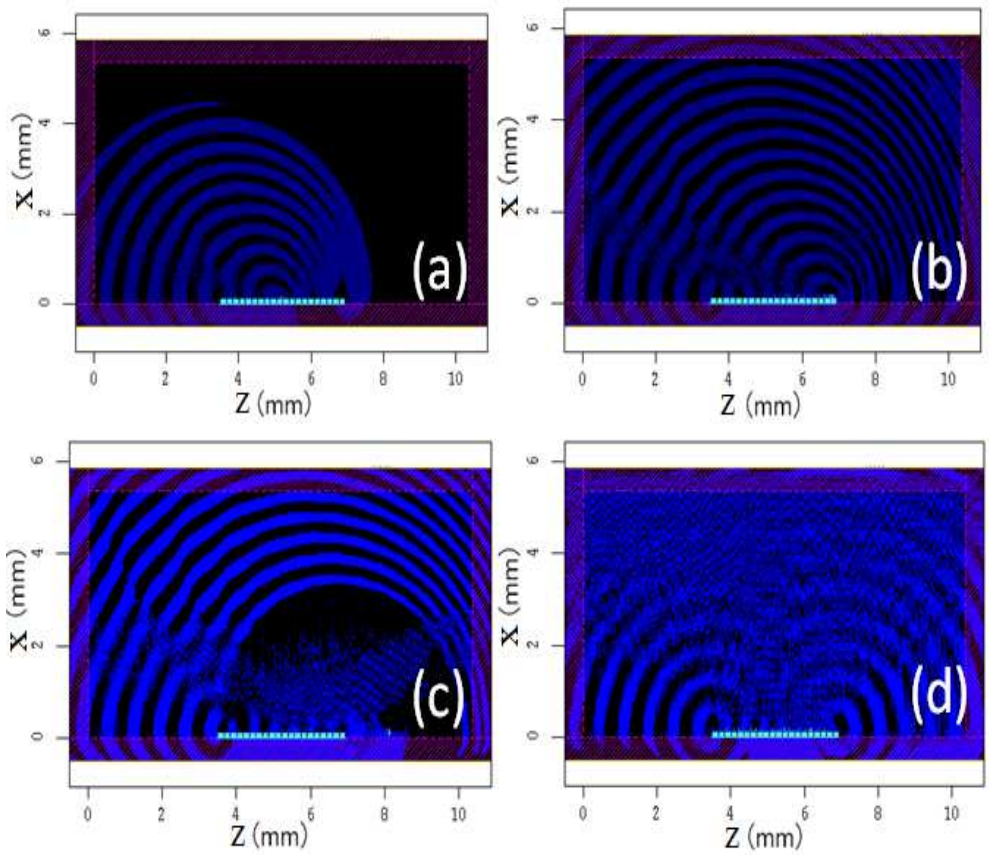

Fig. 6. Contour plots of B_y at (a) t=50.9 ps, (b) t=65.6 ps, (c) t=77 ps, (d) t=148.9 ps

The radiation process can be understood through the contour plots of magnetic field B_y as shown in Fig. 6, where the crescent-shaped wave fronts of the radiation are illustrated. In Fig. 6 (a), we see that the bunch has reached the center of the grating and has covered 10 periods, and 10 crescents clearly appeared in the vacuum box. From this phenomenon we can deduce that the radiation is attributed to Smith-Purcell effect, which has the characteristic that the electron diffracts at every period of grating. Fig. 6(b) shows that the bunch has covered all the periods and has arrived at the end of the grating. From Fig. 6(c) we understand that the Smith-Purcell radiation will no longer be emitted when the bunch moves beyond the grating. But the interesting thing happens in Fig. 6(d), where clear interference pattern appears. It is seen that the pattern is formed by two waves radiated from the two ends of the grating, and we deduce that is the surface wave radiation. The surface wave does not radiate until it reaches the ends of a grating, undergoing partial reflection and partial diffraction. The reflected portion oscillates between the grating's ends, and that is the reason that even the electron bunch disappears from the simulation area the radiation is still emitted.

A set of Bz detectors is placed at the same distance 5.346 mm and various angles from the grating center. One of the temporal behavior observed at 120^o is given in Fig. 7, where again we see that the surface wave oscillates after the Smith-Purcell radiation ends. The corresponding FFT of Fig. 7 is as shown in Fig. 8, clearly demonstrating the Smith-Purcell radiation and surface wave signals, respectively. The surface wave frequency is 425 GHz, independent of radiation angle, lower than the allowed Smith-Purcell radiation frequency at any angles. This value may be read from the dispersion relation for the grating, which was developed in last section. The dependence of the Smith-Purcell radiation frequency on the radiation angle is very close to the theoretical calculation from Eq. (2.6), as shown in Fig. 9. Also plotted is the distribution of Bz amplitude in Fig. 9, which shows that the Smith-Purcell radiation is weak at small angle, and it reaches its maximum at about 125^o in this simulation. This result is in agreement with Fig.2.. The amplitude of the surface wave is not plotted for clarity, and hereafter, we only concentrate on the Smith-Purcell radiation.

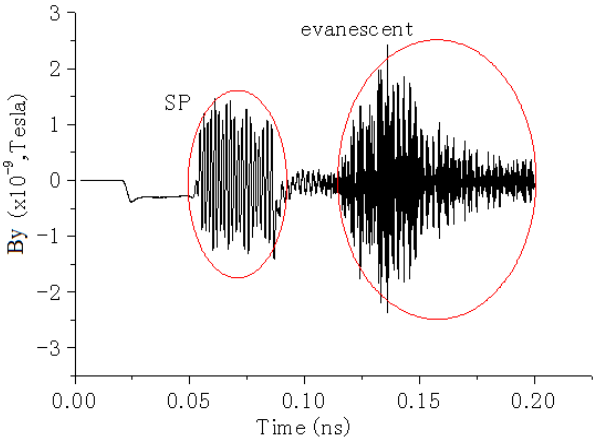

Fig. 7. Time signal of B_y, observed at point 5.346 mm and 120° from the center of the grating.

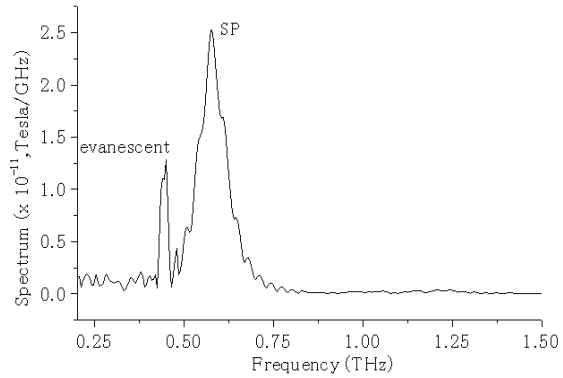

Fig. 8. FFT of time signal corresponding to Fig.7.

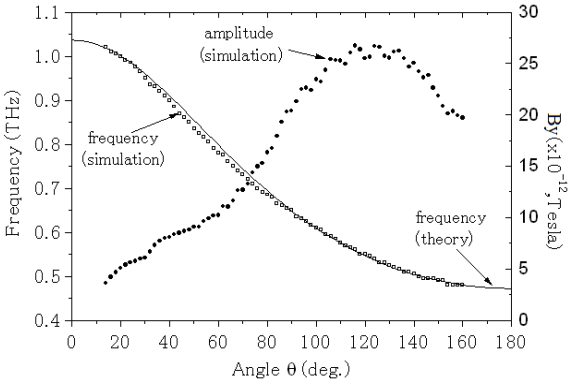

Fig. 9. Radiation frequency and amplitude as a function of angle.

3.2 Train of bunches

When the electron bunches are repeated periodically, the spectral intensity of the radiation is enhanced at the bunching frequency and its harmonics, which is called superradiance. The electron beam can be bunched by some proper devices to form a train of bunches before they are introduced in the grating system. Under certain conditions, a continuous beam can also be bunched by the interaction with the surface wave during its propagation along a grating. In order to clearly demonstrate the properties of superradiant radiation, we generate a train of electron bunches to drive the grating in our simulation.

In this simulation, we also use a grating that has 20 periods. The repeat frequency of bunches is set to be 300 GHz, and the parameters for each single bunch are the same to those mentioned earlier. During the running time, 60 bunches are produced and enter the simulation area. From the FFT of the temporal behavior observed by the Bz detectors we know that the radiation is focused on two frequencies, the second and the third harmonic of bunches' frequency, which falls into the allowed frequency of the first order Smith-Purcell radiation. The results are illustrated in Fig. 10, where two signals are clearly demonstrated.

The dominant radiation is at the second harmonic of bunches' frequency and peaked at the angle 104°, which is the angle satisfying Eq. (2.6) for such a frequency, while the other one radiates at the frequency of the third harmonic, and at the angle of about 40°. Also in Fig. 10, comparing to the second harmonic radiation, the third one is weak, which roughly corresponds to the amplitude distribution shown in Fig. 9. Another evident to prove the fact that the two radiations emit at certain angles can be found in the contour plot of B_y, as shown in Fig. 11. The second harmonic radiation is dominant and clearly observed to radiate at the angle of about 104°, corresponding to what is shown in Fig. 10.

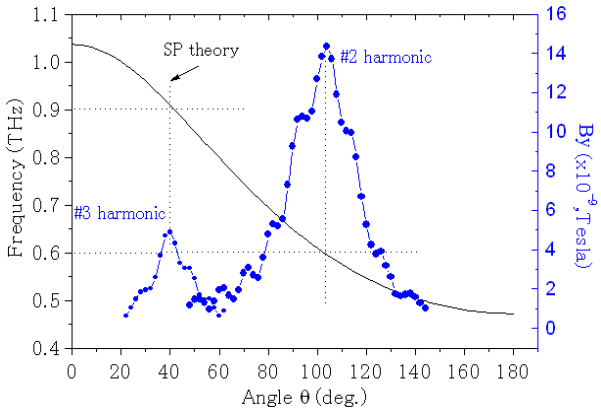

Fig. 10. Amplitude of superradiant radiation as a function of angle. Also shown are the frequency characteristics.

It should be noted that, about the frequency characteristics of superradiant radiation, Andrews and co-workers already predicated in their theoretical analysis[Andrews, H.], and Donohue also discussed it based on the simulation of a continuous beam[Donohue, J.D.]. The results of our pre-bunched beam simulation support their predication.

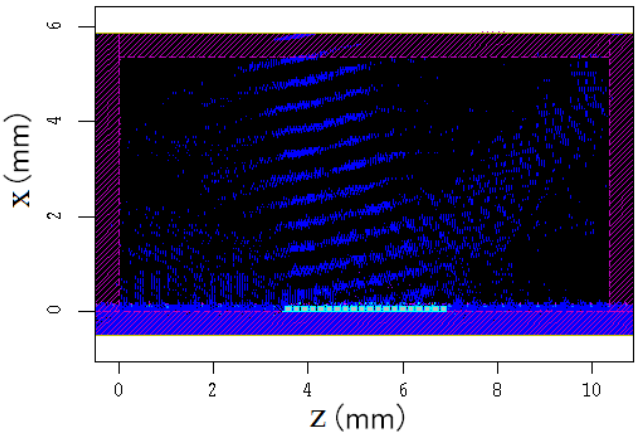

Fig. 11. Contour plot of B_y for superradiant ratiation.

3.3 Continuous beam

The electron beam bunching induced by the surface wave has been addressed by Donohue and Gardelle [Donohue, J.T.]. They also analyzed the relation of growth rate with the electron beam current. Here, we only concentrate on the output power of Smith-Purcell radiation

In this simulation we deal with a grating with 50 periods. The electron beam from the cathode is continuous, not modulated, and an external magnetic field of 2T is introduced to prevent the beam from diverging. We vary the beam current and observe the total power flow out the top plane. From the theoretical analysis in section 2.1, we know that the beam line intersects the dispersion curve at a point representing a backward wave, which means the device operates in the mode of backward-wave oscillator (BWO). Under certain conditions, the device can start to oscillate without external feedback if the beam current exceeds a threshold value beyond gain occurs. During the simulation, we experienced that there surely exists a certain value for the beam current, over which the beam bunching can occur. We read the peak power of Smith-Purcell radiation through the observation of power spectrum, and plot the result in Fig. 12, where we can easily identify two regimes for incoherent and superradiant radiation, respectively. We can also deduce the threshold of beam current.

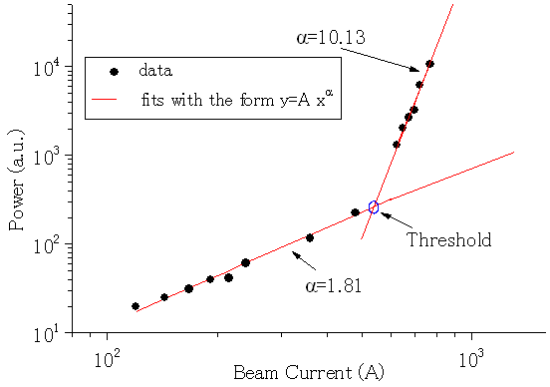

Fig. 12. Output power with respect to the beam current.

The frequency characteristic is given in Fig. 13. It is seen that the frequencies of the incoherent radiation and superradiant radiation are completely different. We found that the frequency of incoherent radiation shows classical Smith-Purcell radiation characteristics, and the 640 GHz shown in Fig. 13 is close to the radiation frequency emitted at 90o, while the superradiant radiation frequency 840 GHz is the second harmonic of the evanescent wave which bunches the beam, independent of radiation angle, and it corresponds to the characteristic discussed earlier. We note that the frequency slightly decreases as the beam current increases, because the space charge reduces the electrons' velocity. The velocity reduction influences the frequency of incoherent and superradiant radiation in different ways: for the case of incoherent radiation, the lower velocity will give rise to lower frequency determined by Eq. 2.6; while for the case of superradiant radiation, the reduction of particle velocity makes the intersection of beam line and dispersion curve shift to smaller frequency (see Fig.4), which means a decrease of the frequency of the surface wave.

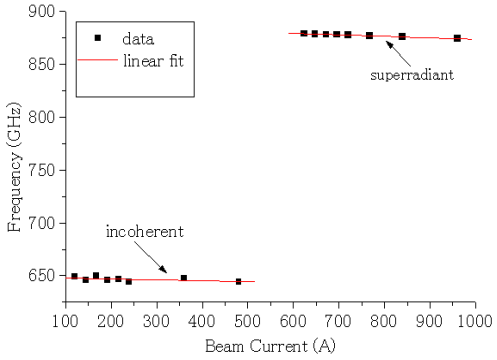

Fig. 13. Frequencies of incoherent and superradiant radiation with respect to beam current.

4. Improvement of Smith-Purcel free-electron laser

In order to improve the efficiency of Smith-Purcell free-electron laser, some new schemes have been worked out. Here we introduce two methods. By those methods, the beam-wave interaction can be enhanced, and then the growth rate could also be improved and, consequently, the start current is expected to be reduced.

4.1 Grating with Bragg reflectors

Based on the fact that the surface wave cannot radiate and it is partially reflected and partially diffracted at the ends of the grating , a scheme of grating with Bragg reflectors is proposed to improve the reflection coefficient, as shown in Fig. 14. For the case of operation point being at the backward-wave region, the Bragg reflector may correspond to the zero harmonic or the -1th harmonic. The reflected zero (or -1^{st}) harmonic increases the entire field when the phase is well matched, and certainly this leads to the increase of the field of zero harmonic and, consequently, the beam-wave interaction would be enhanced. We can tune the lengths of g_1 and g_2 as shown in Fig.14 to optimize the phase-matching. In the following, we demonstrate the scheme of reflecting -1^{st} order harmonic by a two-dimensional particle-in-cell simulation.

The simulations are carried out with using CHIPIC code, which is a finite-difference, time-domain code designed to simulate plasma physics processes. The grating system is assumed to be perfect conductor, and it has uniform rectangular grooves along the y direction, with parameters mentioned above. The main grating is assumed to have 60.5 periods. A sheet electron beam with the thickness of 24 μm propagates along the z direction, and its bottom is over the grating surface by height of 34 μm. It is a perfect beam produced from a small cathode located at the left boundary of the simulation area. The beam wave interaction and radiation propagation occur in the vacuum box, which is enclosed with absorber regions. Since it is a two-dimensional simulation, it is assumed that all fields and currents are independent of the y direction. We have simulated the reflection effect of a surface wave by the end of grating and by Bragg grating with using the method mentioned somewhere[Andrews, H.]. It has been shown that for the frequency of our interest the

reflection coefficient can be improved from 0.35 to 0.85 when a Bragg grating is connected with the end of the main grating, and 10 periods of the Bragg grating is enough.

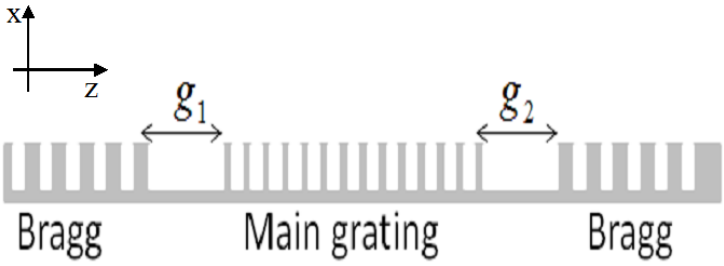

Fig. 14. A scheme of a main grating with Bragg gratings connected at both ends

We firstly determine the wavelength of the -1st order harmonic through simulating the main grating alone, and with using 35 keV electron beam it turns out to be $\lambda_{-1} = 599.2\mu m$, thus, the period of the corresponding Bragg grating should be $d_B^{-1} = \lambda_{-1}/2 = 299.6\mu m$. We simplify choose the groove width as $d_B^{-1}/2 = 149.8\mu m$, and groove depth is 100μm same as that of the main grating. The frequency of the surface wave is 432 GHz, which is a little bit lower than that of the analytical calculation, due to the decrease of the electron's energy induced by the effect of space charge. The procedure of optimization is as follows: since the energy carried by -1st harmonic moves backward (negative z direction), we firstly set the Bragg grating at the upstream end only, and tune g_1 to find the biggest growth rate through observation of the evolution of the y-component magnetic field. The observation point is set 17.3 μm above the grating surface at the center of the main grating; Next, we set another Bragg grating at the downstream end and optimize g_2. The simulation result is shown in Fig. 15, where the evolution of the y-component magnetic field is given.

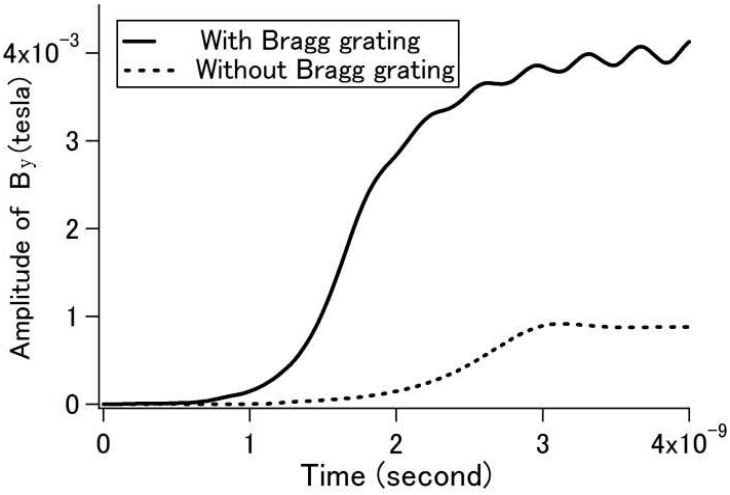

Fig. 15. Evolution of the amplitude of y-component magnetic field.

For comparison, the result obtained without Bragg gratings is also plotted. It is found that for the same current density (1.7×10^6 A/m^2), oscillation starts earlier when Bragg reflectors are used, and saturation occurs sooner. It is found that the growth rate is $\mathrm{Im}(\omega)=4.12\times10^9$ s^{-1} when Bragg reflectors are used and $\mathrm{Im}(\omega)=2.32\times10^9$ s^{-1} when they are not. Bragg reflectors increase the growth rate by a factor of 1.8. By varying the current density it is found that the start current density is 0.9×10^6 A/m^2 when Bragg reflectors are used and 1.6×10^6 A/m^2 when they are not used. Bragg reflectors reduce the start current by a factor of 1.8.

4.1 Grating with sidewall

A sidewall grating is proposed to enhance the coupling of the optical beam with the electron beam. By such a way, the requirements on the electron beam is possible to be relaxed; the growth rate could be improved and consequently the start current could be reduced. It is expected that the optical beam is confined between the two sidewalls to keep a good coupling with the electron beam during the interaction. Furthermore, such a configuration adds no impact on the super-radiant Smith-Purcell emission, which emits over the grating at a certain angle relative to the direction of electron beam propagation, because there is not a top plane above the grating. With the help of three-dimensional particle-in-cell simulations, we compare the general grating (without sidewall) with the sidewall grating and then show the advantages of the latter one.

The simulation models for the general grating and sidewall grating are shown in Fig. 16 (a) and (b), respectively. A cylindrical electron beam is supposed to fly over the grating.

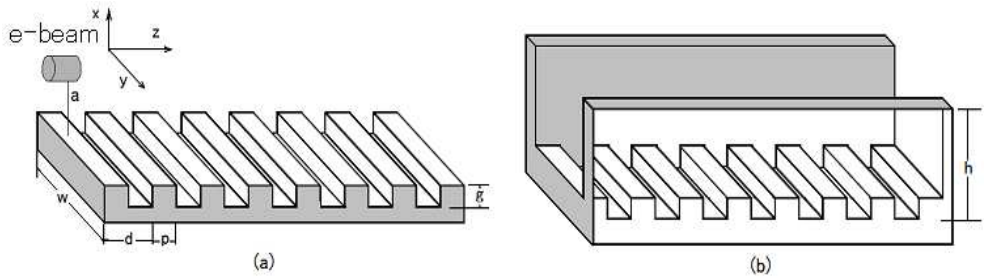

Fig. 16. Schematic of grating model. (a) general grating (b) sidewall grating.

Main parameters are summarized here: period d=2 cm, ridge width p=1 cm, groove depth g=1 cm, grating width w=10 cm, beam hight a=2mm, beam radius r=2.5 mm, beam energy E= 100 keV, wall hight h=14 cm and period number N=46. By these parameters the device operates as a backward wave oscillator, and the synchronous evanescent wave is with the frequency of 4.5 GHz. Details can be found in our previous work[Li, D.]. The grating, assumed to be a perfect conductor, is set in the center of the bottom of a vacuum box bounded by an absorption region. A continuous beam produced from a cathode moves in

the *z*-axis. The simulation area is divided into a mesh with a rectangular cell of very small size in the region of beam propagation and large in the rest. The simulation is performed in the gigahertz region for the convenience to run the code, and we believe the physics applies to the terahertz regime.

The result of the beam-wave interaction is directly reflected by the evolution of the electromagnetic field of the evanescent wave, such as the longitudinal component of electric field Ez. When certain conditions are satisfied, the electric field Ez indicates the processes from spontaneous radiation, exponential growth to saturation. In Fig. 17, the comparisons for the general and sidewall gratings are given. For the case of 0.5 A electron beam, the general grating device cannot reach the saturation even over 500 ns while the sidewall grating device saturates at about 110 ns; for the case of 0.6 A electron beam, the general grating device saturates at around 400 ns while the sidewall grating device saturates at 90 ns. Apparently, the time required to get saturation is dramatically reduced. Furthermore, by the sidewall grating the amplitude of the electric field is also improved.

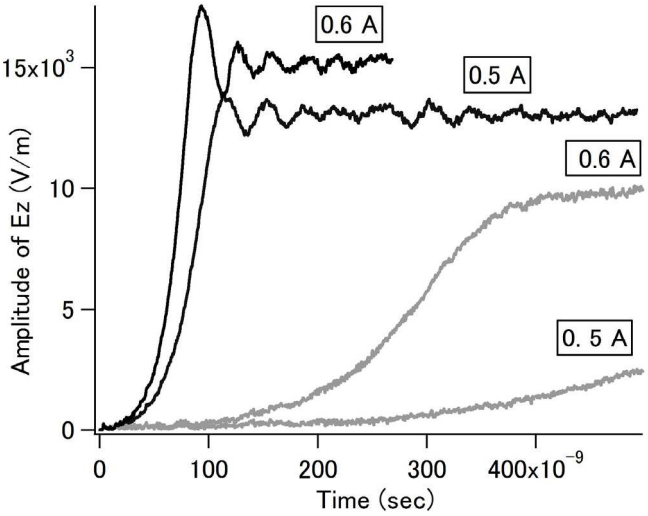

Fig. 17. Evolution of amplitude of electric field Ez. (gray curves for general grating and black curves for sidewall grating.)

5. Grating of negative-index material

There is currently interest on the research of negative-index material, which shows many exotic and remarkable electromagnetic phenomena, such as reversed Cherenkov radiation and reversed Doppler shifts[Agranovich, V. M.]. Recent successes in fabricating these artificial materials [Shelby, R. A.] have initiated an exploration into the use of them to investigate new physics and to develop new applications. It has been demonstrated in theoretical analysis and simulation that enhanced diffraction can be achieved from a grating with negative-index material compared with a grating with positive-index material when a plane-wave is incident [Depine, R. A.]. And this implies a possibility of realizing a high-performance Smith-Purcell free-electron laser.

5.1 Smith-Purcell radiation

We calculate the two-dimensional Smith-Purcell radiation from a grating with a homogeneous, isotropic, and linear material. The grating is with a sinusoidal profile $x = g(z) = 0.5h\cos(\frac{2\pi}{d}z)$, where d is the period and h the amplitude, as shown in Fig.18. The region $x > g(z)$ is vacuous, whereas the medium occupies the region $x < g(z)$, characterized by relative permittivity ε_r and permeability μ_r. If the medium is of the negative-index material, the real part of both permeability and permittivity is negative. And the positive-index material requires that the real part of both permittivity and permeability are positive. The incident wave is supposed to be from a line charge with q coulombs per length passing above the grating with the distance x_0 and velocity v along z-axis. Only considering the TM mode, the y-directed component of magnetic field of the evanescent

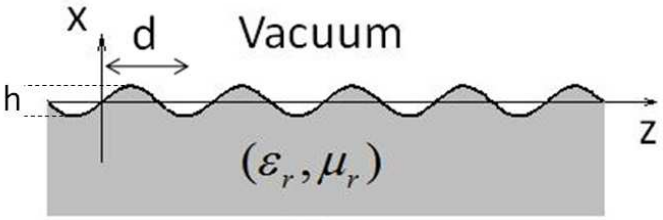

Fig. 18. Schematic diagram of grating

wave from the line charge is given by $\frac{q}{2}e^{\varsigma_0(x-x_0)}e^{j\frac{\omega}{v}z}$ (Hereafter the time part $e^{-j\omega t}$ is omitted), where $\varsigma_0 = \sqrt{\frac{\omega^2}{v^2} - \frac{\omega^2}{c^2}}$, ω the angular frequency, c the light velocity in vacuum. The diffracted and refracted fields by the grating can be represented by Rayleigh expansions, so, the y-directed component of the total magnetic field outside the corrugations can be written as

$$H_y^{(1)} = \frac{q}{2}e^{\varsigma_0(x-x_0)}e^{j\frac{\omega}{v}z} + \sum_{p=-\infty}^{\infty} A_p e^{j\alpha_p x}e^{jk_p z} \quad x > \max g(z) \tag{5.1}$$

$$H_y^{(2)} = \sum_{p=-\infty}^{\infty} B_p e^{-j\beta_p x}e^{jk_p z}, x < \min g(z) \tag{5.2}$$

Here, A_p and B_p are scalar coefficients to be determined and

$$k_p = \frac{\omega}{v} + \frac{2p\pi}{d},\ \alpha_p = \sqrt{\frac{\omega^2}{c^2} - k_p^2},\ \beta_p = \sqrt{\frac{\varepsilon_r\mu_r\omega^2}{c_2} - k_p^2}.$$

For the vacuous half-space the conditions $\mathrm{Re}(\alpha_p) > 0$ and $\mathrm{Im}(\alpha_p) > 0$ are required, whereas the medium half-space requires $\mathrm{Re}(\beta_p) > 0$ for positive-index material, $\mathrm{Re}(\beta_p) < 0$ for negative-index material, and $\mathrm{Im}(\beta_p) > 0$. The corresponding electric fields can be achieved from Maxwell equations. The continuity of the tangential components of the total electric

field and magnetic field at the boundary $x = g(z)$ requires $H_y^{(1)} = H_y^{(2)}$ and $\vec{n} \cdot \nabla H_y^{(1)} = \varepsilon_r^{-1} \vec{n} \cdot \nabla H_y^{(2)}$, where $\vec{n}$ is a unit vector normal to the boundary. According to the Rayleigh hypothesis we assume that the expansions in Eqs.(5.1-5.2) can be used in the boundary conditions. We multiply both sides of a boundary condition by $e^{jk_r z}$ and then integrate with respect to z over one period. After some algebraic works, we obtain a system of linear equations as

$$\sum_{p=-\infty}^{\infty} -A_p \cdot U_{r-p}^p + B_p \cdot V_{r-p}^p = \frac{qe^{-\varsigma_0 x_0}}{2} T_r \tag{5.3}$$

$$\sum_{p=-\infty}^{\infty} A_p \cdot \frac{\frac{\omega^2}{c^2} - k_p k_r}{\alpha_p} \cdot U_{r-p}^p + B_p \cdot \frac{\frac{\varepsilon_r \mu_r \omega^2}{c^2} - k_p k_r}{\varepsilon_r \beta_p} \cdot V_{r-p}^p$$

$$= -\frac{jqe^{-\varsigma_0 x_0}}{2} \cdot \frac{\frac{\omega^2}{c^2} - \frac{\omega}{v} \cdot k_r}{\varsigma_0} \cdot T_r \tag{5.4}$$

where

$$U_{r-p}^p = \frac{1}{d} \int_0^d e^{j\alpha_p g(z)} e^{-j\frac{2\pi(r-p)z}{d}} dz$$

$$V_{r-p}^p = \frac{1}{d} \int_0^d e^{-j\beta_p g(z)} e^{-j\frac{2\pi(r-p)z}{d}} dz$$

$$T_r = \frac{1}{d} \int_0^d e^{\varsigma_0 g(z)} e^{-j\frac{2\pi r z}{d}} dz$$

If the grating is made of perfect conductor, the equations can be simplified as

$$\sum_{p=-\infty}^{\infty} A_p \cdot \frac{\frac{\omega^2}{c^2} - k_p k_r}{\alpha_p} \cdot U_{r-p}^p = -\frac{jqe^{-\varsigma_0 x_0}}{2} \cdot \frac{\frac{\omega^2}{c^2} - \frac{\omega}{v} \cdot k_r}{\varsigma_0} \cdot T_r \tag{5.5}$$

As is known, when the integer p is negative, there exist radiating modes, so called Smith-Purcell radiation. The radiation frequency is dependent on the observation angle and electron velocity, and it can be known from the dispersion relation $k_p = \frac{\omega}{c} \cos\theta_p = \frac{\omega}{v} + \frac{2p\pi}{d}$, where θ_p is measured from electron moving direction. The diffraction coefficient A_p can be worked out through solving the equations numerically. In order to be independent of influence from charge q, we define the radiation factor as $R_p = A_p \big/ (\frac{1}{2} qe^{-\varsigma_0 x_0})$.

Some computations are carried out and the radiated flux $|R_{-1}|^2$ in the -1st-order radiating wave as a function of the observation angle θ_{-1} for 35 keV electrons are given in Fig. 19 and Fig. 20. In Fig.19, comparing with the positive-index material ($\varepsilon_r = 5$, $\mu_r = 1$), it is shown that the radiated flux is higher in the region from $\pi/2$ to π for the negative-index material

($\varepsilon_r = -5$, $\mu_r = -1$), which means strong radiation can be obtained. In Fig. 20, we plot the cases of negative-index material and perfect conductor. Comparing with the perfect conductor, the negative-index material shows strong radiation in the region from $\pi/4$ to $3\pi/4$, while outside this region the radiation from the perfect conductor predominates.

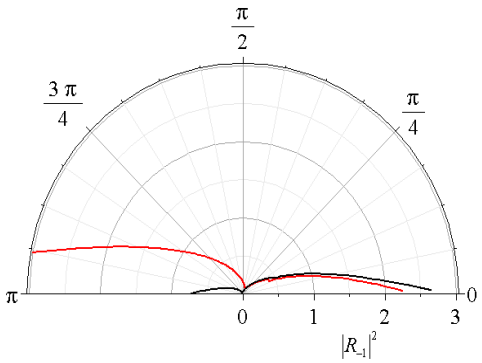

Fig. 19. Radiated flux $|R_{-1}|^2$ as a function of the observation angle θ_{-1} for 35 keV electrons. Grating period d =1 mm, h/d =0.1. (Red line for negative-index material $\varepsilon_r = -5$, $\mu_r = -1$. Black line for positive-index material $\varepsilon_r = 5$, $\mu_r = 1$)

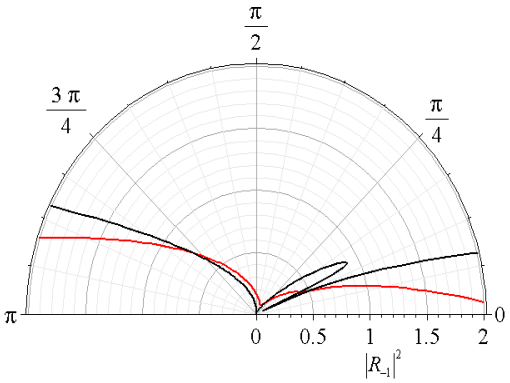

Fig. 20. Radiated flux $|R_{-1}|^2$ as a function of the observation angle θ_{-1} for 35 keV electrons. Grating period d =1 mm, h/d =0.1. (Red line for negative-index material $\varepsilon_r = -5$, $\mu_r = -1$. Black line for perfect conductor)

5.2 Surface wave

We have known that the surface modes of a grating play an important role in the operation of a Smith-Purcell free-electron laser[Andrews, H., Li, D]. The continuous electron beam interacts with the surface mode and is bunched periodically when beam current is beyond so called start current, then the periodic bunches emits in the form of super-radiant Smith-Purcell radiation at a certain angle. Next, we explore the surface mode of a grating with negative-index material.

Considering the case of without incident wave, there are only evanescent wave near the corrugation boundary. Thus, the y-directed component of the total magnetic field outside the corrugations can be written as

$$H_y^{(1)} = \sum_{m=-\infty}^{\infty} C_m e^{-\alpha_m x} e^{jk_m z} \ , \ x > \max g(z) \tag{5.6}$$

$$H_y^{(2)} = \sum_{m=-\infty}^{\infty} D_m e^{\beta_m x} e^{jk_m z} \ , \ x < \min g(z) \tag{5.7}$$

Here, C_m and D_m are scalar coefficients and

$$k_m = k + \frac{2m\pi}{d} \ , \ \alpha_m = \sqrt{k_m^2 - \frac{\omega^2}{c^2}} \ , \beta_m = \sqrt{k_m^2 - \frac{\varepsilon_r \mu_r \omega^2}{c^2}} \ .$$

For the vacuous half-space the conditions $\mathrm{Re}(\alpha_m) > 0$ and $\mathrm{Im}(\alpha_m) < 0$ are required, whereas the medium half-space requires $\mathrm{Re}(\beta_m) > 0$, $\mathrm{Im}(\beta_m) > 0$ for negative-index material, and $\mathrm{Im}(\beta_m) < 0$ for positive-index material. Using the same boundary conditions mentioned above, it is straightforward to get a system of linear equations as

$$\sum_{m=-\infty}^{\infty} -C_m \cdot F_{n-m}^m + D_m \cdot G_{n-m}^m = 0 \tag{5.8}$$

$$\sum_{m=-\infty}^{\infty} C_m \cdot \frac{\frac{\omega^2}{c^2} - k_m k_n}{\alpha_m} \cdot F_{n-m}^m + D_m \cdot \frac{\frac{\varepsilon_r \mu_r \omega^2}{c^2} - k_m k_n}{\varepsilon_r \beta_m} \cdot G_{n-m}^m = 0 \tag{5.9}$$

where

$$F_{n-m}^m = \frac{1}{d} \int_0^d e^{-\alpha_m g(z)} e^{-j\frac{2\pi(n-m)z}{d}} dz$$

$$G_{n-m}^m = \frac{1}{d} \int_0^d e^{\beta_m g(z)} e^{-j\frac{2\pi(n-m)z}{d}} dz$$

The dispersion relation for surface mode is obtained by equating to zero the determinant of the coefficients in these equations. Through numerically calculating we get the dispersion curve for negative-index material ($\varepsilon_r = -9$, $\mu_r = -0.1$) and ($\varepsilon_r = -0.1$, $\mu_r = -11$) as is shown in Fig. 21. The 35 keV beam line is also plotted, and the intersection implies the operation point, where the surface wave is synchronous with electron beam. It is also shown that the 35 keV electron beam interacts with the backward-wave, thus, the external feedback system is not necessary. If the beam current is high enough for a device to oscillate, the electron beam would be periodically bunched, and those periodic bunches can emit at the second harmonic in the form of super-radiant Smith-Purcell radiation [Andrews, H., Li, D.].

The permittivity ε_r and permeability μ_r are limited in a narrow region, $(-1 < \mu_r < 0, -1 > \varepsilon_r > 1/\mu_r)$ and $(\mu_r < -1, -1 < \varepsilon_r < 1/\mu_r)$, for the existence of surface wave. However, this limitation can be relaxed by placing a conductor boundary at the bottom of the grating. Such a grating scheme is under research.

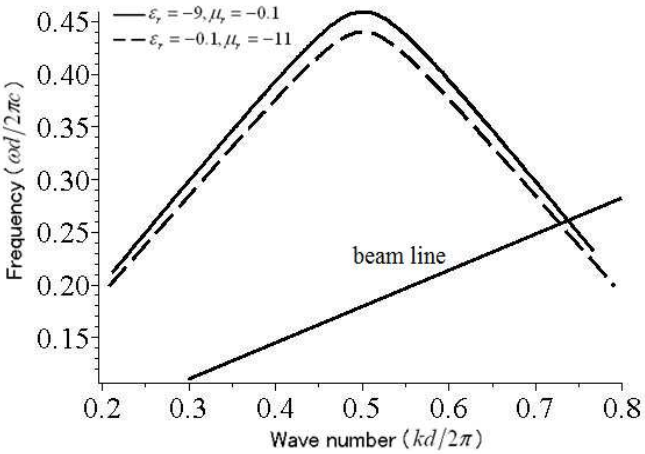

Fig. 21. Dispersion relation of surface waves from the grating of negative-index materials.

6. Conclusion

In conclusion, we theoretically analyzed the the Smith-Purcell radiation and the surface waves induced on the surface of a grating. The evanescent wave of a moving charge is reflected by the periodic structure on the surface of a grating, and the radiating part in the reflected waves forms the Smith-Purcell radiation. The grating also supports surface wave, which plays an important role in the operation of a Smith-Purcell free-electron laser. The surface wave cannot radiate, but it interacts with the electron beam and realize periodic beam bunch, resulting in the generation of super-radiant Smith-Purcell radiation. These phenomena are demonstrated with the help of particle-in-cell simulation. The sidewall grating and Bragg reflection system are proposed to improve the efficiency of Smith-Purcell free-electron laser. Both of them can enhance the beam-wave interaction, improve the growth rate and reduce the start current, which are promissing technologies in the development of Smith-Purcell free—electron lasers. We explored the grating made of negative-index materials, and find that in a certain range of radiation angle the Smith-Purcell radiation is stronger than that from a grating made of metal or positive-index materials. The surface wave from such a grating is also invegistated, which shows possibility in developing a Smith-Purcell free-electron laser.

7. Acknowledgment

This work is supported by a Grant-in-Aid for Scientific Research on Innovative Areas "Electromagnetic Metamaterials" (No. 22109003) from The Ministry of Education, Culture, Sports, Science, and Technology (MEXT), Japan.

8. References

Agranovich, V.M.; Gartstein, Yu. N. (2006). Spatial dispersion and negative refraction of light, *Physics-Uspekhi*, Vol. 49, No. 10, pp.1029-1044.

Andrews, H.; Brau, C.A. (2004). Gain of a Smith-Purcell free-electron laser, *Physical Review Special Topics - Accelerators and Beams*, Vol. 7, pp. 070701-1-070701-7. (2009). Observation of THz evanescent waves in a Smith-Purcell free-electron laser, *Physical Review Special Topics - Accelerators and Beams*, Vol. 12, pp. 080703-1-080703-5.

Chen,H.-T; Padilla,W.J., Zide,J.M.O., Gossard,A.C. & Taylor, A.J. (2006). Active terahertz metamaterial devices, *Nature*, Vol. 444,597-600.

Depine, R. A.; Lakhtakia, A. (2004). Plane-wave diffraction at the periodically corrugated boundary of vacuum and a negative-phase-velocity material, *Physical Review E*, Vol. 69, pp.057602-1-057602-4

Donohue, J.T.; Gardelle, J. (2006). Simulation of Smith-Purcell terahertz radiation using a particle-in-cell code, *Physical Review Special Topics - Accelerators and Beams*, Vol. 9, pp. 060701-1-060701-7. (2005). Simulation of Smith-Purcell radiation using a particle-in-cell code, *Physical Review Special Topics - Accelerators and Beams*, Vol. 8, pp. 060702-1-060702-9.

Gardelle, J.; Modin, P. & Donohue, J.T. (2010). Start Current and Gain Measurements for a Smith-Purcell Free-Electron Laser, *Physical Review Letters*, Vol. 105, No. 26, pp. 224801-1-224801-4. (2009). Observation of coherent Smith-Purcell radiation using an initially continuous flat beam, *Physical Review Special Topics - Accelerators and Beams*, Vol. 12, pp. 110701-1-110701-6.

Gover, A.; Livni Z. (1978). Operation Regimes of Cerenkov-Smith-Purcell Free Electron Lasers and T.W. Amplifiers, *Optics Communications*, Vol. 26, No. 3, pp. 375-380

Kuma, V.; Kim, K. J. (2006). Analysis of Smith-Purcell free-electron lasers, *Physical Review E*, Vol. 73, pp. 026501-1-026501-15.

Leavitt, R.P.; Wortman, D. E. & Morrison C.A. (1979). The orotron-A free-electron laser using the Smith-Purcell effect, *Applied Physics letters*, vol. 35, pp.363-365.

Li, D.; Yang, Z., Imasaki, K. & Park, G. S. (2006). Particle-in-cell simulation of coherent and superradiant Smith-Purcell radiation, *Physical Review Special Topics - Accelerators and Beams*, Vol. 8, pp. 060702-1-060702-9. Vol. 9, pp. 040701-1-040701-6. (2006). Three-dimensional simulation of super-radiant Smith-Purcell radiation, *Applied Physics Letters*, Vol. 88, pp. 201501-1-201501-2. (2011). Improve growth rate of Smith–Purcell free-electron laser by Bragg reflector, *Applied Physics Letters*, Vol. 98, pp. 211503-1-211503- 3

Schächter, L.; Ron, A. (1989). Smith-Purcell free-electron laser, *Phys. Rev. A,* Vol. 40, No.2, pp.876-896.

Shelby ,R.A.; Smith,D.R.& Schultz,S. (2011). Experimental Verification of a Negative Index of Refraction, *Science*, Vol. 292, 77-79.

Shelby, R. A.; Smith, D. R. & Schultz, S. (2001). Experimental erification of anegative index of refraction, *Science*, Vol. 292, pp. 77-79.

Shibata, Y.; Hasebe, S., Ishi, K., Ono, S. & Ikezawa, M. (1998). Coherent Smith-Purcell radiation in the millimeter-wave region from a short-bunch beam of relativistic electrons, *Physical Review E*, Vol. 57, No. 1, pp. 1061-1074

Smith, S. J.; Purcell, E. M. (1953). Visible Light from Localized Surface Charges Moving across a Grating, *Phys. Rev. ,* Vol.92, pp. 1069-1069.

van den Berg, P.M. (1973); Smith-Purcell radiation from a line charge moving parallel to a reflection grating, *Journal of the Optical Society of America*, Vol. 63, No. 6, pp.689-698

Walsh, J.; Woods, K. & Yeager, S. (1994). Intensity of Smith-Purcell radiation in the relativistic regim, *Nuclear Instruments and Methods in Physics Research A*, Vol. 341, pp. 277-279

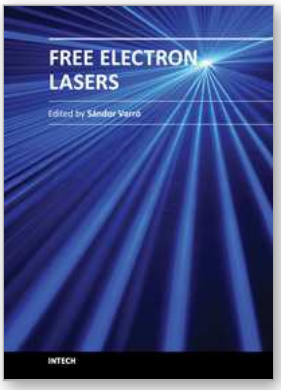

Free Electron Lasers
Edited by Dr. Sandor Varro

ISBN 978-953-51-0279-3
Hard cover, 250 pages
Publisher InTech
Published online 14, March, 2012
Published in print edition March, 2012

Free Electron Lasers consists of 10 chapters, which refer to fundamentals and design of various free electron laser systems, from the infrared to the xuv wavelength regimes. In addition to making a comparison with conventional lasers, a couple of special topics concerning near-field and cavity electrodynamics, compact and table-top arrangements and strong radiation induced exotic states of matter are analyzed as well. The control and diagnostics of such devices and radiation safety issues are also discussed. Free Electron Lasers provides a selection of research results on these special sources of radiation, concerning basic principles, applications and some interesting new ideas of current interest.

InTech Europe
University Campus STeP Ri
Slavka Krautzeka 83/A
51000 Rijeka, Croatia
Phone: +385 (51) 770 447
Fax: +385 (51) 686 166
www.intechopen.com

InTech China
Unit 405, Office Block, Hotel Equatorial Shanghai
No.65, Yan An Road (West), Shanghai, 200040, China
中国上海市延安西路65号上海国际贵都大饭店办公楼405单元
Phone: +86-21-62489820
Fax: +86-21-62489821